Article

A Model Study of the Discharges Effects of Kaidu River on the Salinity Structure of Bosten Lake

Ying Liu [ID]**, Anming Bao *, Xi Chen and Ruisen Zhong**

State Key Laboratory of Desert and Oasis Ecology, Xinjiang Institute of Ecology and Geography,
Chinese Academy of Sciences, Urumqi 830011, China; lyhello@yeah.net (Y.L.); chenxi@ms.xjb.ac.cn (X.C.);
risen2008@foxmail.com (R.Z.)
* Correspondence: baoam@ms.xjb.ac.cn; Tel.: +86-991-7885378

Abstract: The salinization of Bosten Lake, which is the largest lake in the arid or semi-arid region of Xinjiang, has increased. To study the effects of the inflow change of Kaidu River, the main recharge, on the salinity structure of Bosten Lake, the Estuarine, Coastal, and Ocean Modeling System with Sediments (ECOMSED), a basic three-dimensional numerical model, was used. The model is forced by realistic atmospheric forcing and river inflows, and verified by observational data. The model simulations can map the lake water movement processes and offer an understanding of the likely role of river runoff on the Bosten Lake salinity structure. The water mainly flows eastward at the surface and westward at the bottom. The river runoff of Kaidu River significantly affects the salinity structure of the southwestern part of the lake. The Kaidu River discharge mostly flowed northeastward along the west bank of the lake, so with decreasing Kaidu River discharge, the salinity of the region from the inlet of the river to its right (looking in the direction of the flow) subsequently increased. This study helps to the mastering of the dynamic change of salinity and provides some quantity information for controlling the salinization of Bosten Lake.

Keywords: Bosten Lake; Kaidu River; salinity; ECOMSED

1. Introduction

Water salinization in arid and semi-arid areas is a common problem [1] that has occurred in Ebinur Lake, the largest saltwater lake in Xinjiang, northwestern China; the Aral Sea and Balkhash Lake, located in the arid regions of Central Asia; Sambhar Lake, located in an arid region of Rajasthan, India; and the Great Salt Lake, the largest lake in Utah, USA [2]. Water is not suitable for drinking when its salinity is higher than 1.5 g L^{-1}, and cannot be used for irrigation or industrial purposes when its salinity is higher than 2.0 g L^{-1} [2].

The impacts of salinization of water are significant, increasing, harmful, and largely irreparable [3]. The environmental, social, and economic costs of water salinization are high [3]. Salinization of lake water affects industry expenditures, agriculture productivity, and the health of people, animals, and environment [4–8]. Some ecological costs are a substitution of halotolerant species for halosensitive biota, changes in the characteristics of aquatic ecosystems, decreased biodiversity, productivity reduction, soil salinization, and decreasing of usable water resources [3].

Bosten Lake is situated in the southern part of Xinjiang: the arid and semi-arid region of northwestern China. It is the largest lake in Xinjiang, and was the largest inland freshwater lake in China before the 1960s. However, it has changed from a freshwater to a slightly saline lake [9,10]. Bosten Lake water salinization must be controlled to meet the high demand for water resources in the surrounding arid region, and for conserving the environment around the lake [2].

Nowadays, many inland waters are salinizing due to human activities, especially in arid and semi-arid regions [3]. The water is salinizing due to a combination of diversion and damming of upstream rivers, extensive land use changes, saline agricultural drainage, saline wastewater dumping, and discharge of shallow saline groundwater in arid and semi-arid regions [11–16]. Bosten Lake is salinizing due to its geographical location which has high evaporation, very low precipitation, high salinity content of the surrounding soil, large-scale excessive utilization and exploitation of water resources in the source areas, reduction of discharge, and increasing saline agricultural return flow into the lake [17–19].

Bosten Lake water salinization has attracted the attention of the government, communities and scholars. Many past researches of the salinization of the lake treated it as a black box and calculated its average salinity using mathematical methods or constructing salt water balance equations to analyze its change based on spatially sparse observed data [2,20–23]. The horizontal salinity distributions in Bosten Lake have been studied using zone analysis from observed data or two-dimensional numerical methods and models [24,25]. However, given the remarkably irregular boundary line and highly variable bottom topography, which significantly affects the physical processes, three-dimensional salinity models have great advantages in simulating the salinity of Bosten Lake. Although Bosten Lake salinization has been reported and studied by many scholars, little work has been done to show the three-dimensional salinity structure and the impacts of the discharge of Kaidu River on the salinity structure of Bosten Lake. It is important to see the effect of the inflow of Kaidu River on the Bosten Lake circulation and then salinity structure in detail as Kaidu River is the major discharge of the increasingly salinized Bosten Lake and controls its salinization process. Kaidu River contributes 83.4% of the total inflow into the lake [26], and the temporal change of salinity of Bosten Lake parallels the discharge of Kaidu River into the lake.

The main aim of this paper is to examine the salinity structure of Bosten Lake and the response of the salinity structure of Bosten Lake to Kaidu River discharge using a three-dimensional numerical model, the terrain-following Estuarine, Coastal, and Ocean Modeling System with Sediments (ECOMSED). Our study is motivated by an increasing demand for preventing the lake water from increasing salinization. This study provides information on how the discharge of Kaidu River influences the salinity structure of Bosten Lake and for mitigating the salinization of Bosten Lake in the future. It may also provide some insights about changing our water utilization and exploitation mode in arid or semi-arid regions.

The paper is arranged as follows. The next section briefly introduces the model and its inputs. In Section 2 we validate the model using in situ observational data. Section 4 gives the model results and Section 4 gives five experiments that analyze the effects of the discharge of Kaidu River on the salinity structure of Bosten Lake. The last section gives the conclusions.

2. Methods

2.1. The Study Area

Bosten Lake is located between 41°56′ N to 42°14′ N and 86°40′ E to 87°56′ E. It is the largest lake in Xinjiang and was previously the largest inland freshwater lake in China. It is at the foot of southern Tian-Shan Mountains, on the northeastern rim of the Taklimakan Desert/Tarim Basin, and in the southern part of Xinjiang, an arid and semi-arid area in western China, and is a Mesozoic fault lake situated in a depression of the western zone of folded strata in the Tian-Shan Mountains [22]. The length and width of the lake is, on average, 55 km from east to west, and approximately 20–25 km from south to north, respectively. When the lake water level is 1048 m a.m.s.l., its water area is 1160 km^2, its storage capacity is 8.41×10^9 m^3, and its average and maximum water depth is 8.1 m and 15 m, respectively. The lake is very shallow near the shores and deepest in its east-central part with an asymmetrical bottom topography [27]. Bosten Lake gets water inflow from a 56,000 km^2 catchment area [28]. More than 10 rivers and small streams recharge Bosten Lake. The most important perennial

tributary of Bosten Lake is Kaidu River, occupying ~83.4% of its total water inflow. Other significant tributaries are the Huangshuigou, the Qing-Shui River, and Wu-La-Si-Te River [29]. The Kaidu River's total length, catchment area, and average annual runoff volume are 513 km, 2.2×10^4 km^2, and 3.412×10^9 m^3, respectively. In the lake, there is only 68.2 mm annual precipitation, primarily falling throughout the summer months, and as high as an approximately 1800–2000 mm annual potential evaporation rate, and 8.4 °C mean annual temperature [26]. Winds come primarily from the southwest, manifesting predominant impact of the westerlies during the summer season. The mean residence time of the lake water is 1731 days with salinity ranges between 0.2 and 2.5 g L^{-1} [30,31]. The salinity of the Bosten Lake water rose from 0.6 g L^{-1} in 1958 to 1.87g L^{-1} in 1988, decreased to 1.12g L^{-1} in 2002, increased again, and is presently ~1.3 g L^{-1}. Since the 1970s, its water salinity has been commonly over 1.0 g L^{-1} [17]. The lake has become a slight saltwater lake since 1958 due to human activities [20].

It is the head of the Kongque River and the end of the Kaidu River (Figure 1). It plays a significant role in controlling floods from the upstream Kaidu River and providing water for the downstream Kongque River Watershed and the lower reach of Tarim River, which provides drinking water for more than 1.3 million people and water for industry, agriculture, and the ecosystem of its ~50,000 km^2 downstream watershed. The lake water source is important for the economic development and societal stability of southern Xinjiang, and also is the main water resource for the endangered vegetation in the downstream of the Tarim River Basin: it is the lifeblood of Xinjiang [32].
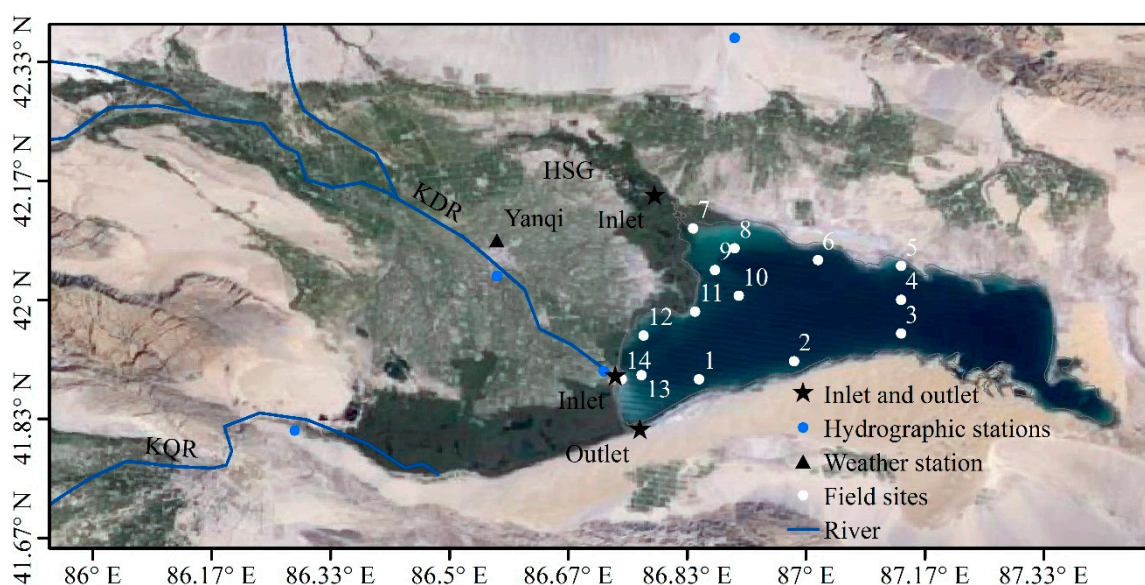
Figure 1. The surroundings (obtained from Google Earth) and topography of Bosten Lake (where white sold circles stand for the measured sites; KDR, KQR, and HSG represent Kaidu River, Kongque River, and Huangshuigou, respectively; and the black stars stand for the inlets of KDR and HSG, and the outlet to KQR).

2.2. Model Description

The three-dimensional Estuarine, Coastal, and Ocean Modeling System with Sediments (ECOMSED) was adopted to study the salinity structure in Bosten Lake. ECOMSED was developed from the Princeton Ocean Model [33] and its version named ECOM for shallow water environments—rivers, bays, estuaries, the coastal ocean, reservoirs, and lakes [34]. The model is designed to provide a realistic parameterization of the vertical mixing processes through incorporating a turbulence closure model [35]. An orthogonal curvilinear coordinate system is used in ECOMSED, greatly increasing model efficiency in treating irregularly shaped coastlines and a sigma (terrain following) vertical coordinate system is used, having doubtless advantages in dealing with big bathymetric irregularities, such as when bottom topographical slopes are large. It has been demonstrated to be reliable and robust over the years [36].

The predictive capabilities of the model have been evaluated via far-ranging comparisons with observed data and a confidence has been built that the dominant physics are actually reproduced by the model. The detailed description of the ECOMSED is in its users' manual [36].

Consider a system of orthogonal Cartesian coordinates with x increasing eastward, y increasing northward, and z increasing vertically upwards. The free surface is located at $z = \eta(x,y,t)$ and the bottom is at $z = -H(x,y)$. If is the horizontal velocity vector with components (U,V) and ∇ the horizontal gradient operator, the continuity equation is

$$\nabla \cdot \overline{V} + \frac{\partial W}{\partial z} = 0,$$ (1)

The Reynolds momentum equations are

$$\frac{\partial U}{\partial t} + \overline{V} \cdot \nabla U + W \frac{\partial U}{\partial z} - fV = -\frac{1}{\rho_0} \frac{\partial P}{\partial x} + \frac{\partial}{\partial z} \left(K_M \frac{\partial U}{\partial z} \right) + F_x,$$ (2)

$$\frac{\partial V}{\partial t} + \overline{V} \cdot \nabla V + W \frac{\partial V}{\partial z} + fU = -\frac{1}{\rho_0} \frac{\partial P}{\partial y} + \frac{\partial}{\partial z} \left(K_M \frac{\partial V}{\partial z} \right) + F_y,$$ (3)

$$\rho g = -\frac{\partial P}{\partial z},$$ (4)

where $\overline{V}$ is the horizontal velocity vector with eastward and northward components (U, V), W is the vertical velocity, P is the pressure, K_M is the vertical eddy diffusivity of turbulent momentum mixing, f is a latitudinal variation of the Coriolis parameter, F_x and F_y are the eastward and northward horizontal diffusivities terms, ρ_0 is the reference density, ρ is the in situ density, and g is the gravitational acceleration. At surface,

$$\rho_0 K_M \frac{\partial}{\partial z} \left(\frac{\partial U}{\partial z}, \frac{\partial V}{\partial z} \right) = \left(\tau_{ox}, \tau_{oy} \right),$$ (5)

and in the bottom layer

$$\rho_0 K_M \frac{\partial}{\partial z} \left(\frac{\partial U}{\partial z}, \frac{\partial V}{\partial z} \right) = \left(\tau_{bx}, \tau_{by} \right),$$ (6)

where $\left(\tau_{ox}, \tau_{oy} \right)$ are the eastward and northward surface wind stress components and $\left(\tau_{bx}, \tau_{by} \right)$ are the eastward and northward bottom friction stress components.

$$\overline{\tau_0} = \rho_0 C_D |V_0| V_0,$$ (7)

$$\overline{\tau_b} = \rho_0 C_d |V_b| V_b,$$ (8)

where C_D is the drag coefficient at surface, C_d is the drag coefficient in the bottom layer.

The conservation equations for salinity may be written as

$$\frac{\partial S}{\partial t} + \overline{V} \cdot \Delta S + W \frac{\partial S}{\partial z} = \frac{\partial}{\partial z} \left[K_H \frac{\partial S}{\partial z} \right] + F_s,$$ (9)

where S is the salinity, K_H is the vertical eddy diffusivity for turbulent mixing of salt, and F_s is the horizontal diffusivity term.

The vertical mixing coefficients, K_M and K_H, are obtained by appealing to a second order turbulence closure scheme [35] which characterizes the turbulence by equations for the turbulence kinetic energy, $q^2/2$, and a turbulence macroscale, l, according to,

$$\frac{\partial q^2}{\partial t} + \overline{V} \cdot \nabla q^2 + W \frac{\partial q^2}{\partial z} = \frac{\partial}{\partial z} \left(K_q \frac{\partial q^2}{\partial z} \right) + 2K_M \left[\left(\frac{\partial U}{\partial z} \right)^2 + \left(\frac{\partial V}{\partial z} \right)^2 \right] + \frac{2g}{\rho_0} K_H \frac{\partial \rho}{\partial z} - \frac{2q^3}{B_1 l} + F_q,$$ (10)

$$\frac{\partial(q^2 l)}{\partial t} + \overline{V}\cdot\nabla(q^2 l) + W\frac{\partial(q^2 l)}{\partial z} = \frac{\partial}{\partial z}\left[K_q\frac{\partial}{\partial z}(q^2 l)\right] + lE_1 K_M\left[\left(\frac{\partial U}{\partial z}\right)^2 + \left(\frac{\partial V}{\partial z}\right)^2\right] + \frac{lE_1 g}{\rho_0}K_H\frac{\partial \rho}{\partial z} - \frac{q^3}{B_1}\widetilde{W} + F_l, \quad (11)$$

where F_q and F_l are the horizontal mixing and $\widetilde{W}$ is a wall proximity function.

The specific difference scheme and solution steps of the governing equations refer to Blumberg and Mellor (1980) [37].

A computational domain of the model ranges from approximately $41°56'$ N to $42°14'$ N and $86°40'$ E to $87°56'$ E covering the big lake of Bosten Lake as displayed in Figure 1. In the horizontal direction, an orthogonal curvilinear grid is used to map the domain in 144×67 grid cells with a resolution of 550 m $\times$ 550 m. There are 11 sigma levels of uniform thickness. The model comprises $144 \times 67 \times 11$ computational grid points (Figure 2). In the vertical direction, a staggered grid is designed with an implicit numerical scheme.
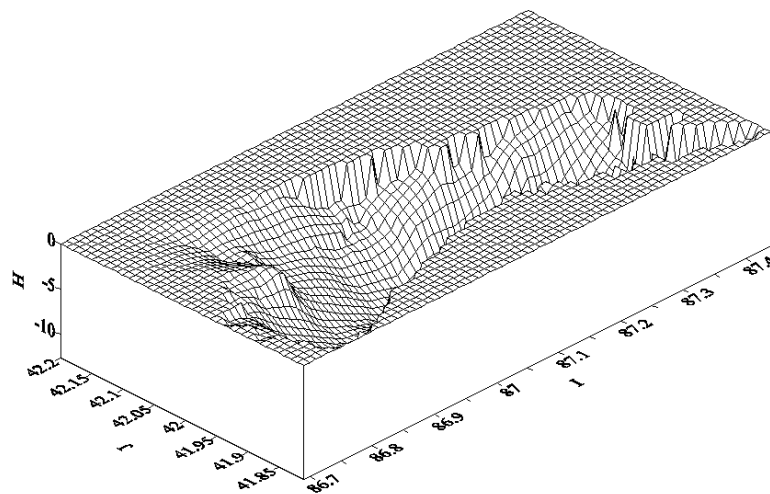
Figure 2. The computational grids for the model showing every second model grids point.

A mode-splitting technique in time is employed. The two different time steps are 120 s for the internal mode and 12 s for the external mode, determined by the conventional Courant–Friedrichs–Lewy (CFL) stability criterion as follows

$$\Delta t \leq \frac{1}{C_t}\left(\frac{1}{\Delta x^2} + \frac{1}{\Delta y^2}\right)^{-1/2}, \quad (12)$$

$$C_t = 2(gH)^{1/2} + \overline{U}_{max}, \quad (13)$$

where $\overline{U}_{max}$ is the maximum average velocity expected and Δx and Δy are the gird size.

In the model we set the horizontal eddy viscosity and diffusivity coefficient of 1.0×10^{-1} m^2/s for the horizontal mixing scheme of Smagorinsky (1963) [38], and the vertical viscosity and diffusivity coefficient of 1.0×10^{-6} m^2/s for the vertical mixing scheme of Mellor-Yamada (1982) [35]. The drag coefficient in the bottom layer set to 3.6×10^{-3}. In this study, we used two types of external forcing to drive the circulation model: surface wind forcing and heat flux at the surface; and buoyancy forcing connected with runoff into Bosten Lake. At the surface boundary, because there are no more meteorological measurements around the lake to get the spatial structures of the wind forcing, the wind forcing over Bosten Lake is assumed spatially homogeneous and equal to the wind forcing calculated from hourly wind velocity data at the 10 m height at Yanqi Station at the eastern bank of Bosten Lake using the bulk formula of Ahsan and Blumberg (1999) [39]. The rose map of wind direction in the station is shown in Figure 3. Moreover, hourly meteorological data covering air temperature and pressure, relative humidity, rainfall, evaporation, and cloud cover acquired from the China Climatology Meteorological data sharing service system at Yanqi station (Figure 1) were applied in this model to

calculate heat fluxes. The net heat flux of Bosten Lake was also estimated using the bulk formula of Ahsan and Blumberg (1999) [39], which has been proven in the literature to have success in modeling heat budget in reservoirs, inland lakes, and estuarine systems (Blumberg, 2002) [36].
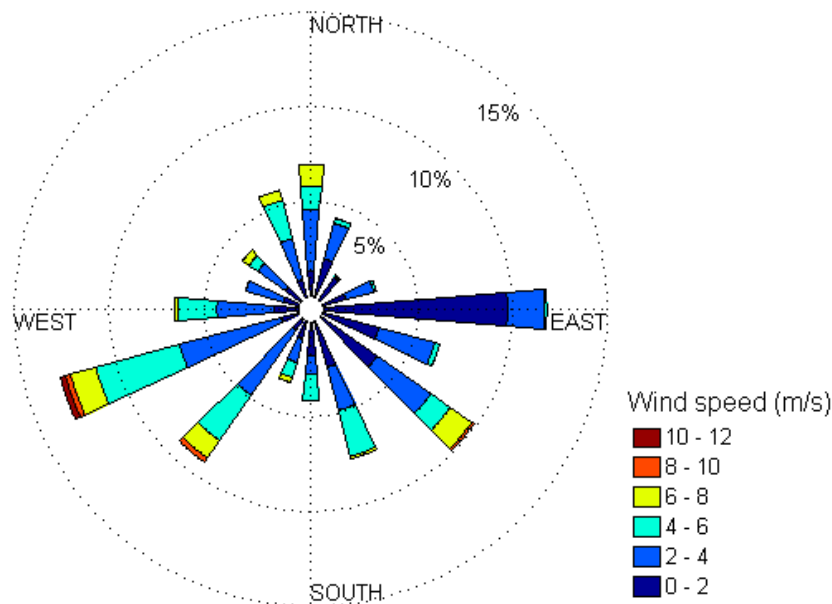
Figure 3. Wind rose map.

Because of the unavailability of direct observations of solar radiation at Yanqi Station, Bosten Lake, or nearby regions in 2005, solar radiation as computed by the method of Rosati and Miyakoda (1988) [40] as follows was used and assumed to be uniformly distributed throughout the model domain.

$$H_s = Q_{TOT}(1 - 0.62C + 0.0019\beta)(1 - \alpha),$$ (14)

$$Q_{TOT} = Q_{DIR} + Q_{DIFF},$$ (15)

$$Q_{DIR} = Q_0\tau^{secz},$$ (16)

$$Q_{DIFF} = [(1 - A_\alpha)Q_0 - Q_{DIR}]/2,$$ (17)

$$Q_0 = \frac{J_0}{r^2}\cos z D_F(\phi, \lambda),$$ (18)

$$\sin\beta = \sin\varnothing\sin[23.45\sin(d - 82)] + \cos\varnothing\cos[23.45\sin(d - 82)],$$ (19)

$$\cos z = \sin\varnothing\sin\delta + \cos\varnothing\cos\delta\cos h,$$ (20)

where H_s is the solar radiation incident the water, Q_{TOT} is the total radiation reaching the water surface under clear skies, Q_{DIR} is the direct solar radiation reaching the water surface, Q_{DIFF} is the diffuse sky radiation under cloudless conditions, Q_0 is the radiation at the top of the atmosphere, C is the fractional cloud cover, β is the solar noon altitude in degrees, α is the water surface albedo, τ is an atmospheric transmission coefficient with a value of 0.7, A_α is the water vapor plus ozone absorption with a value of 0.09, J_0 is the solar constant with a value of 1.35×10^2 J m^{-2}s^{-1}, r is the radius of the earth, z is the zenith angle, and D_F is the fraction of daylight which is a function of latitude; d is the Julian day, $\varnothing$ is the latitude, δ is the sun declination angle, and h is the sun's hour angle.

A plentiful of fresh water is discharged into Bosten Lake from several rivers and streams, which prominently influences the density-driven circulation in Bosten Lake. Daily river flow and temperature at Kaidu River, Kongque River, and Huangshuigou were used as the river boundary conditions. Their daily discharges (Figure 4) were obtained from the Hydrological Yearbook of

the People's Republic of China of Inland Rivers and Lakes in the Southern Tian-Shan Mountains, Xinjiang (SLB, 2005) [41]. Some factors are given to let the river flow reflect the real inflow into the lake. For salinity, linear interpolation of some monthly data observed at a nationally-controlled Environmental Monitoring Station was used. Because there were no hydrographic climatology data available for Bosten Lake, the model temperature and salinity fields are initialized with hydrographic measurements made on 5 April 2005 (hydrographic measurements made on 22 June 2005 are applied to validate the model results). The initial data field is interpolated to the model resolution through kriging interpolation. The model initial temperature and salinity (on 5 April 2005) are set to be horizontally heterogeneous and vertically stratified. The horizontal heterogeneity of salinity in Bosten Lake is such that the salinity is low around the south corner of the lake and high around Huangshuigou. The vertical initial model salinities and temperatures over Bosten Lake are similar to those averaged from the observed hydrographic measurements. The initial model currents are set to zero. The model bathymetry is obtained from kriging interpolation of field water depth. The simulation period is from 17 March to 30 November 2005.
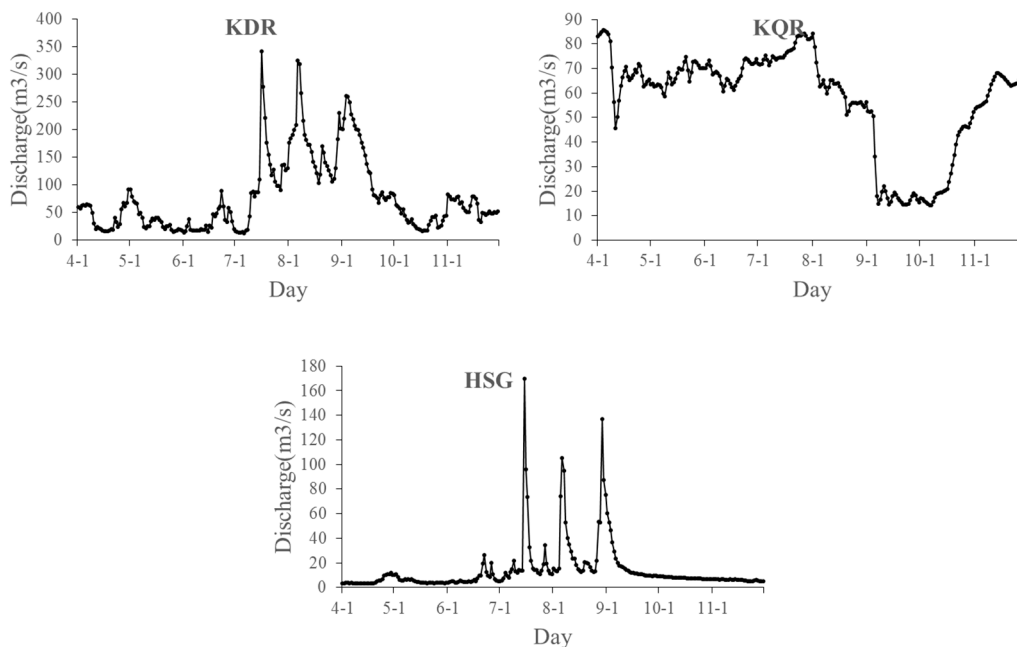
Figure 4. The flow at hydrological stations of Kaidu River (KDR), Huangshuigou (HSG), and Kongque River (KQR) used in driving the model of Bosten Lake during the study period from 00:00 1 April to 00:00 30 November 2005.

Since we are concerned with the impact of the discharge of Kaidu River on the salinity distribution in Bosten Lake, five experiments were designed to study the impact of river discharge on salinity distribution (Table 1). In experiment A1, which is the control run, the model is initialized with the 5 April water column mean salinity and temperature fields and forced by hourly average surface wind stress and heat flux and daily mean flows through the model's river boundaries. Experiments A2–A5 are river discharge experiments. From experiments A1–A5, the response of the salinity structure of Bosten Lake to discharge from Kaidu River can be known. In all numerical experiments, the model simulates without wind stress for 15 days to achieve a quasi-equilibrium state, afterwards the model simulates with wind stress for the rest. Results of five experiments are showed after 98 days of simulation.

Table 1. Model experiments and their conditions.

Experiments	Conditions
A1	Driven by winds from 1 April to 30 November 2005 and daily discharges
A2	Same as A1, but the discharge of Kaidu River is increased by a factor of 0.5
A3	Same as A1, but the discharge of Kaidu River is increased by a factor of 0.25
A4	Same as A1, but the discharge of Kaidu River is decreased by a factor of 0.25
A5	Same as A1, but the discharge of Kaidu River is decreased by a factor of 0.5

3. Results and Discussion

3.1. Model Validation

In order to test the model accuracy, model calibration and verification were conducted using observation data collected in June 2005. We compared the water level, temperature, and salinity simulated by the model to their observed counterparts and found the model has reasonable skill in reconstructing observations. The simulated mean water level 7.46 m is similar to the mean observed 7.43 m. The simulated mean temperature 14 °C is also similar to the water column mean observation data. The simulated salinity was compared with the observed at fourteen sites listed in Figure 1. There is little difference between simulated and observed salinity at the sites (Figure 5), and the observed and modeled salinities have a correlation coefficient (R^2) of 0.87 (Figure 6). The little difference is mainly in sites 7, 9, 10, 11, 12, and 13 which lay at the eastern side of the lake because of the Kaidu River discharge influence and the Huangshuigou influence. Site 7 is in the Huangshuigou region that is the agriculture return flow region with high salinity, site 14 is in the inlet of Kaidu River to the lake, and site 13 around the Kaidu River inlet region.
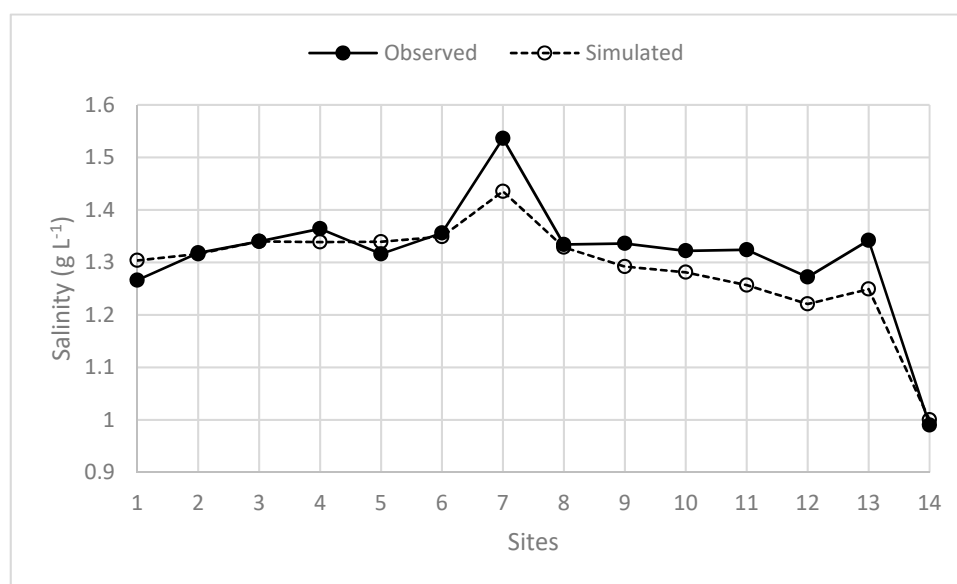
Figure 5. Comparison between observed and modeled salinities at sites 1 to 14 (see Figure 1), where the observed data are marked by filled circles and the simulated results marked by open circles.

In addition, an index of salinity difference ratio (SDR) designed as the ratio of the sum of the squared magnitudes of the salinity differences between the simulated and the observed salinity to the sum of the squared magnitudes of the observed salinities is used for salinity validation, i.e.,

$$SDR = \sum\left(|S_m - S_o|^2\right) / \sum|S_o|^2, \tag{21}$$

where S_o is the observed salinity and S_m is the modeled salinity. The lower the SDR, the better the agreement between the modeled and observed values. When SDR equals 0, this indicates a perfect agreement between the modeled and observed data. In our model results, the maximum SDR is 0.09, which presents that the simulated salinities consist well with the observed data. The model can capture the spatial distribution of salinity.

We also compared the currents simulated by the model to the results of Han et al. (2004) [24]. In general, the modeled currents are similar to the results (Figure 7) of Han et al. (2004) [24]. At the surface, the water flows from the west to east along the northern and southern banks, and flows in the reverse direction in the lake central. The maximum flow velocity is no more than 1.1m/s, and the flow velocity of the lake middle is under 0.3 m/s.
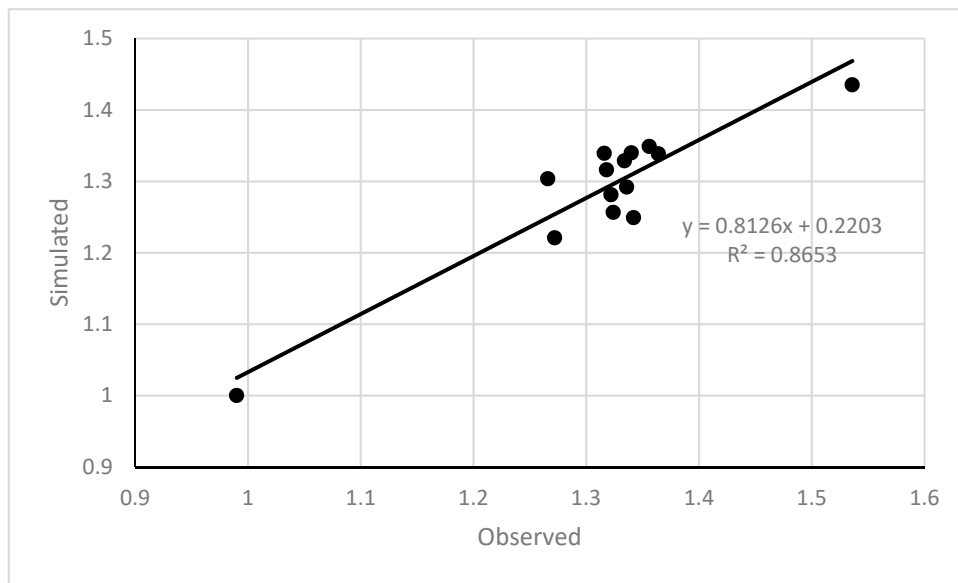
Figure 6. The relationship between the observed and modeled salinities at sites 1 to 14 (see Figure 1).
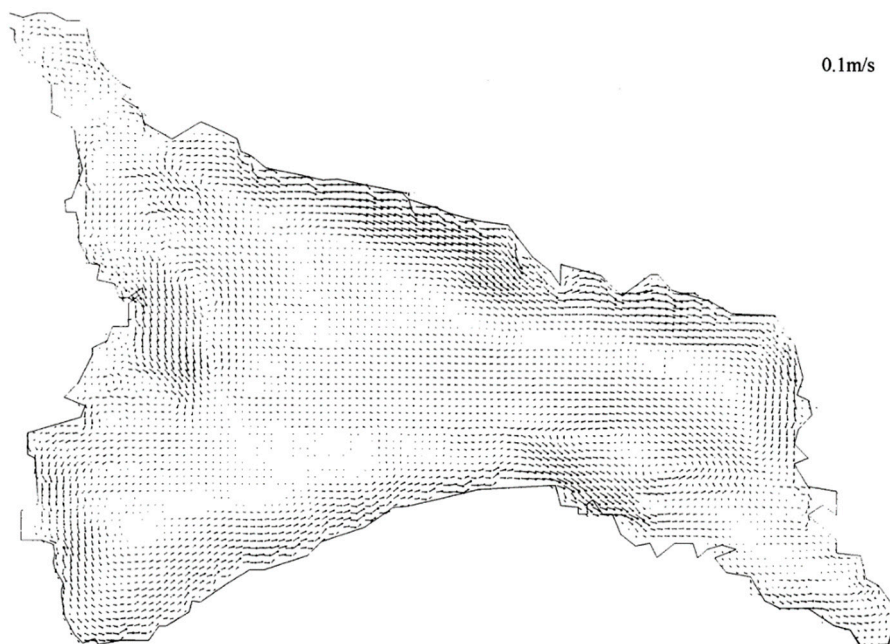
Figure 7. The simulated current results by Han et al. (2004) [24].

The above comparisons suggest that the model is suited to simulate the salinity distribution and study the impacts of the discharge of Kaidu River on the salinity structure of Bosten Lake.

3.2. Analyses of Model Results

In general, the water flows eastward along the south and north shores, flows northeastward and northward along the west and east shores in the surface, but flows westward at the south-central part of the lake in the bottom layer; the current speed at the surface is larger than that in the bottom layer, and the speed of flow along the eastern bank is slower than that along other bank both at the surface and in the bottom layers (Figure 8). At the surface, the speed of flow along the western, northern, and southern shores are larger than that of other regions, and there are small circumfluences at the east-central and southwest-central part and along the eastern shore of the lake (Figure 8(A1-S)). In the bottom layer, the speed of flow in the southern part of the lake is larger than that of the northern part of the lake, due to the fact that the southern part of the lake is deeper than the northern part of the lake. In addition, there are clockwise circumfluences in the northern part of the lake and anticlockwise circumfluences near the southern bank, and some relatively isolated small circumfluences near the shores. In addition, the flow along the bank is weak (Figure 8(A1-B)).
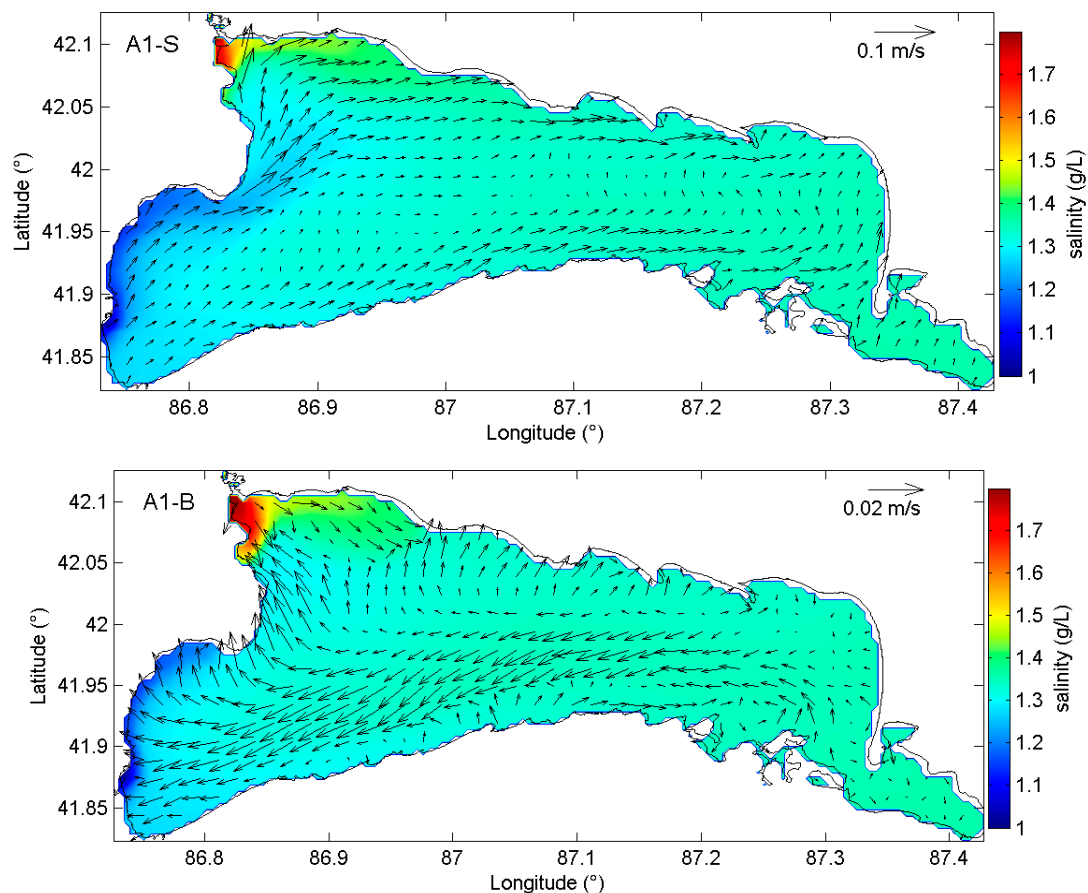
Figure 8. Distribution of simulated residual currents and salinity (**A1-S**) at the surface, and (**A1-B**) in the bottom layer in experiment A1. The simulated currents are shown at every third model grid point.

The simulated salinity is lower in the southwestern part of the lake, especially from around the mouth of Kaidu River to its left along the western bank, and higher in the northwestern part of the lake, especially from around the mouth of Huangshuigou to its left along the northern bank, and of intermediate values at other regions, where the salinity is homogenous (Figure 8). This pattern is mainly due to the freshwater inflow from Kaidu River, and the slightly saline water exists at the

northwestern part of the lake, the historical saline agricultural return flow region, and the weak flow in the middle part of the lake. The minimum salinity in the southwestern part of the lake is also due to outflow to Kongque River through pump stations, and both the inlet from Kaidu River and the outlet to Kongque River exist in the region. The salinity at the surface is lower than that in the bottom layer along the western shore of the southwestern part of the lake, and along the northern bank of the northwestern part of the lake, but is almost same with the bottom in other regions (Figure 8). Moreover, the high salinity region along the northern shore near the Huangshuigou extends further along the north shore at the surface than that in the bottom layer, and the low salinity region of the southwestern part of the lake is larger at the surface than in the bottom layer. This is due to the flow speed of the surface layer is larger than that of the bottom layer, the water flows eastward along the northern bank, and northeastward along the western bank of the lake at the surface (Figure 8(A1-S)). The water flows eastward accounted into some water flows northward at the northern bank of the northwestern part of the lake, and water flows westward at the southwestern part of the lake in the bottom (Figure 8(A1-B)), and then the surface low salinity water at the southeastern part of the lake and the high salinity water at the northern bank of the northwestern part of the lake disperses into a bigger region at the surface than that at the bottom.

To better show the three-dimensional salinity structure of Bosten Lake, three sections were chosen (Figure 9). Section I in the eastward area starts from the inflow of Kaidu River and ends at the east boundary, section II in the northward area starts from the pump station and ends at the north boundary, and section III in the southeastward area starts from the inlet of Huangshuigou, and ends at the south boundary (Figure 9). The salinity along section I is lower around the inlet of Kaidu River, increases eastward, and is high near the bottom and along the eastern boundary (Figure 10(A1-I)). The salinity along section II is high around the pump station and the bottom, decreases northward, and is low along the north boundary (Figure 10(A1-II)). The salinity of the right side of section I and the left side of section II is low are also due to that the freshwater inflow from Kaidu River flows northeastward along the western bank of the lake. In section III, salinity is higher around the inlet of the Huangshuigou and at the bottom, and lower in the middle of section III (Figure 10(A1-III)), which is due to the fact that the northwestern part of the lake is the saline agricultural return flow region, and the freshwater inflow from the Kaidu River flows northeastward resulting in lower salinity in the middle of the lake.
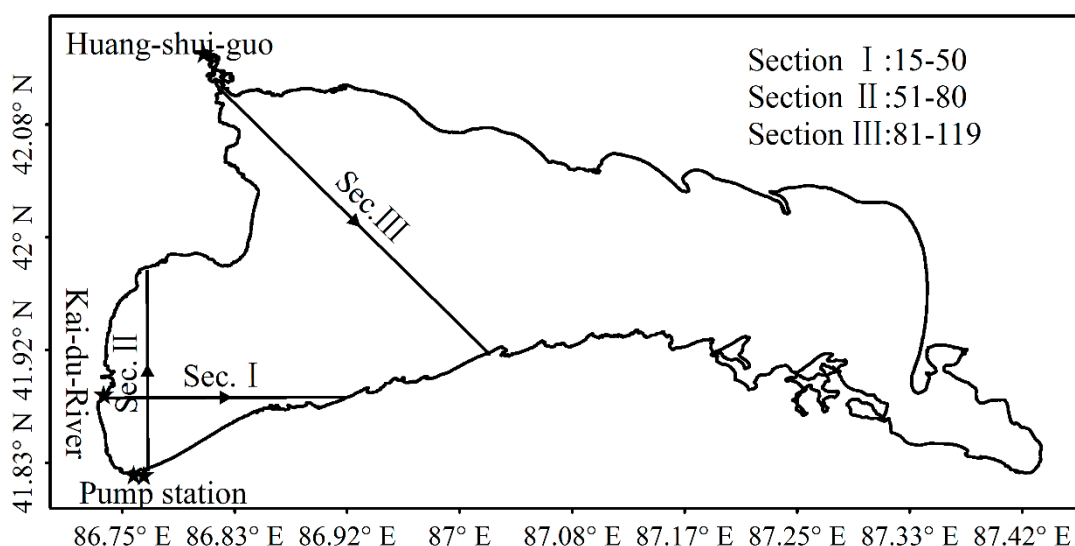
Figure 9. The three sections of Sec.I, Sec.II, and Sec.III were selected to show salinity changes in the sensitivity experiments. The arrows show the direction of the sections.
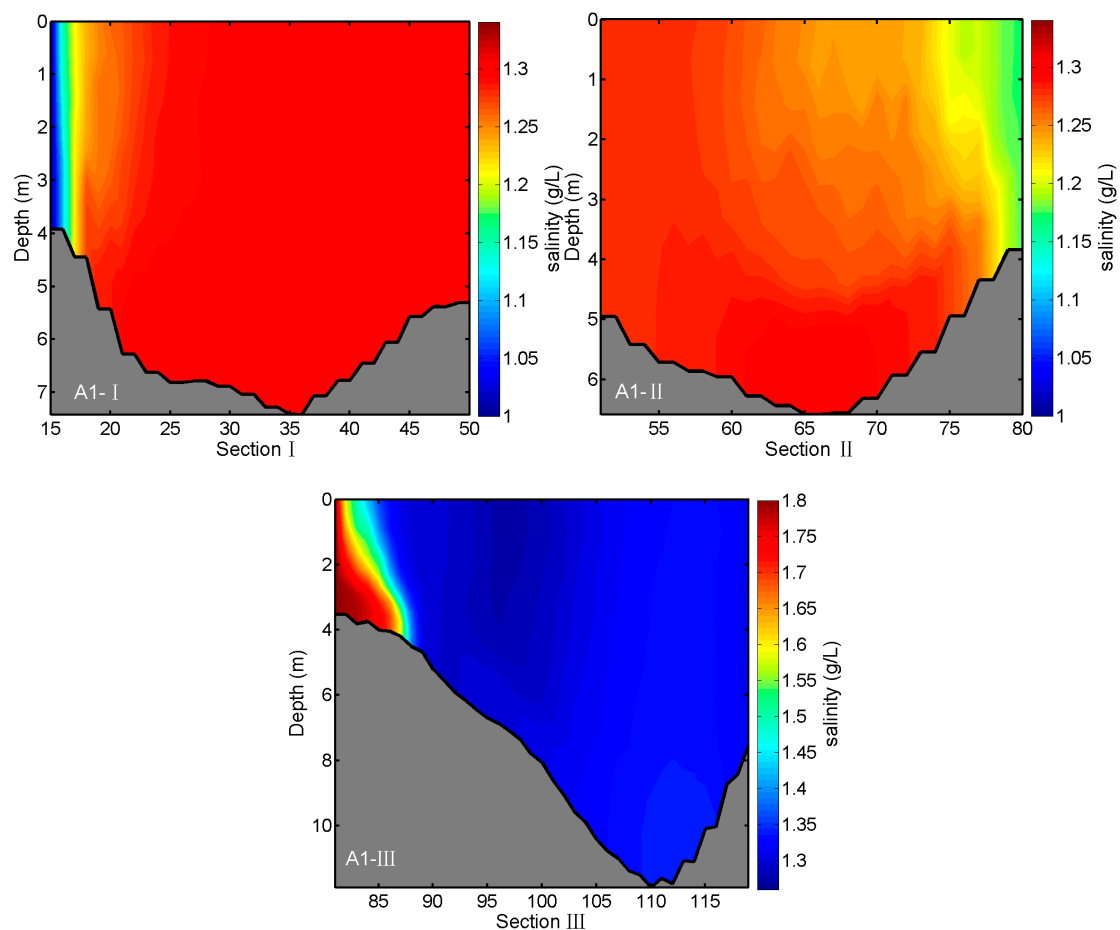
Figure 10. Distribution of modeled salinity at (**A1-I**) Section I, (**A1-II**) Section II, and (**A1-III**) Section III in experiment A1.

3.3. Effects of River Discharges on Salinity Distributions

To study the impact of Kaidu River discharge on the salinity distribution, experiments A2–A5 were set. Experiments A2 and A3 are similar to experiment A1, except the Kaidu River discharge at the inlet increased by 0.5 and 0.25 times, respectively, while the other model settings remain unaltered. Experiments A4 and A5 are also similar to experiment A1, except the Kaidu river discharge at the inlet decreased by 0.25 and 0.5 times, respectively, while the other model settings remain unaltered. The Kaidu River discharge at the inlet in experiments A2, A3, A1, A4, and A5 is decreased, the salinity near the inlet of Kaidu River along the western bank is increased, and the region with a clear salinity gradient in the southwest increases too, especially along the western and southern banks, so that salinity in the southwest lake is increased (Figure 11), and the salinity increases more at the surface than in the bottom layer, which means the decrease in discharge of Kaidu River has a greater impact at the surface than in the bottom layer. The extent of the region with increased salinity is determined by the quantity of the discharge into the lake. In the fiver experiments, due to the water flowing northeastward at the surface and westward at the bottom, the salinity increased along the western bank in the southwest of the lake to a greater degree at the surface than near the bottom. When the river discharge at Kaidu River is decreased in experiments A2, A3, A1, A4, and A5, the location of the 1.25 g L^{-1} isohaline at the surface moves eastward and northeastward (Figure 15(A-S)), which also shows that the salinity increased in the southwest of the lake.
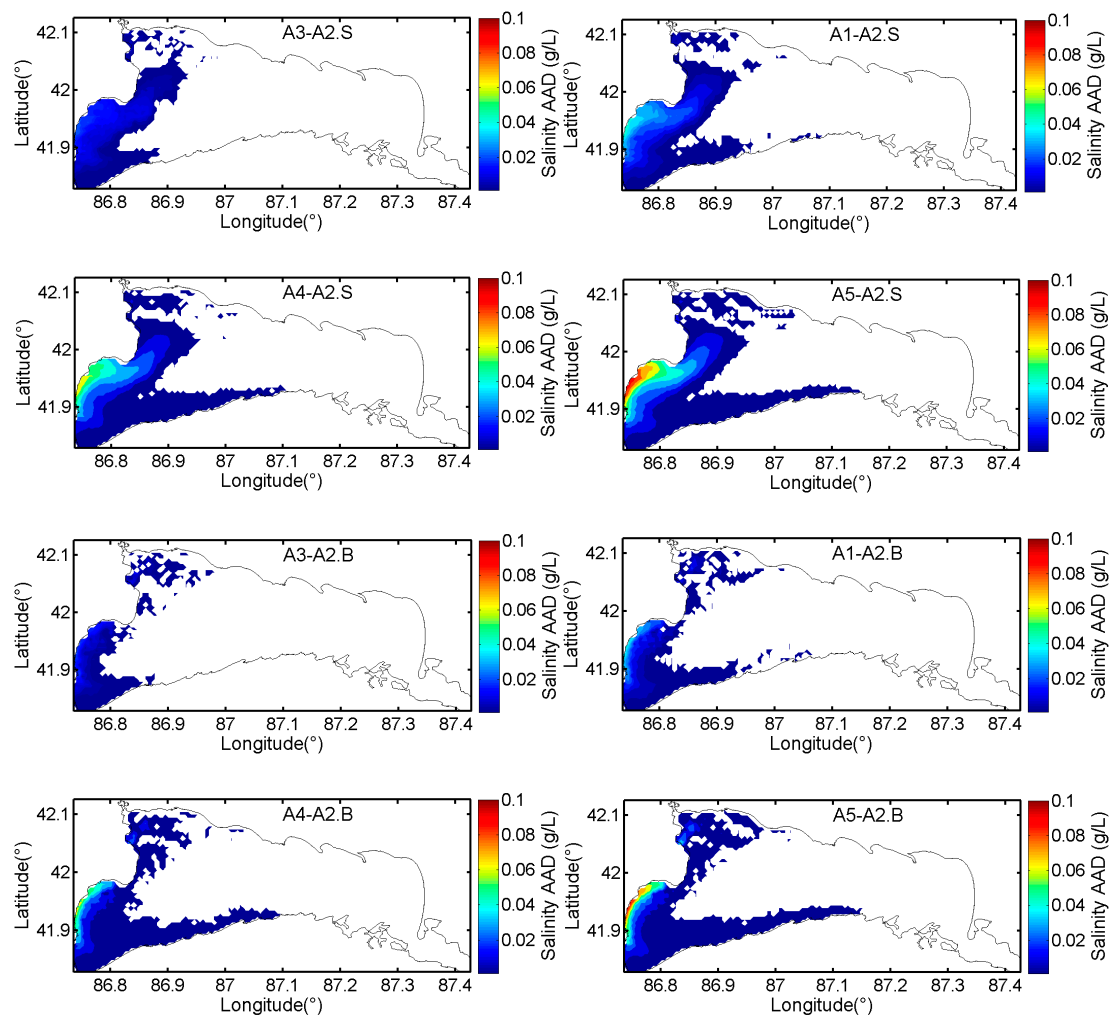
Figure 11. The Salinity average absolute differences (AAD) distributions between experiments at surface (**A3-A2.S**) A3-A2, (**A1-A2.S**) A1-A2, (**A4-A2.S**) A4-A2, and (**A5-A2.S**) A5-A2, and at the bottom (**A3-A2.B**) A3-A2, (**A1-A2.B**) A1-A2, (**A4-A2.B**) A4-A2, and (**A5-A2.B**) A5-A2.

With the decrease in the discharge of Kaidu River, the salinity along section I, section II, and section III was also increased (Figures 12–14). It is obvious that the region with salinity below 1.1 g L^{-1} to the left of section I decreased in size, and the region with salinity above 1.3 g L^{-1} increased in size with the decrease in the discharge of Kaidu River (Figure 12), so that the salinity along section I increased. When the discharge from Kaidu River is decreased in experiments A2, A3, A1, A4, and A5, the location of the 1.25 g L^{-1} isohaline at the surface moves to the western bank (the left of the section) (Figure 15(AI)), which also shows the salinity increased in the southwest of the lake.

The area with salinity below 1.2 g L^{-1} to the right of section II decreased with the decrease in the discharge of Kaidu River (Figure 13), which means the salinity along section II increased, the discharge of Kaidu River has a greater impact on the right of section II, which can be seen in Figure 11 too. When the river discharge at Kaidu River is decreased in experiments A2, A3, A1, A4, and A5, the location of the 1.25 g L^{-1} isohaline at the surface moves apparently to the northern bank (the right of the section) (Figure 15(AII)), which also shows the salinity increased in the southwest of the lake. The discharge of Kaidu River has a greater impact at section II, because most of section II is near the western bank of the southwest of the lake. Kaidu River has a greater influence in the western bank (Figure 11).
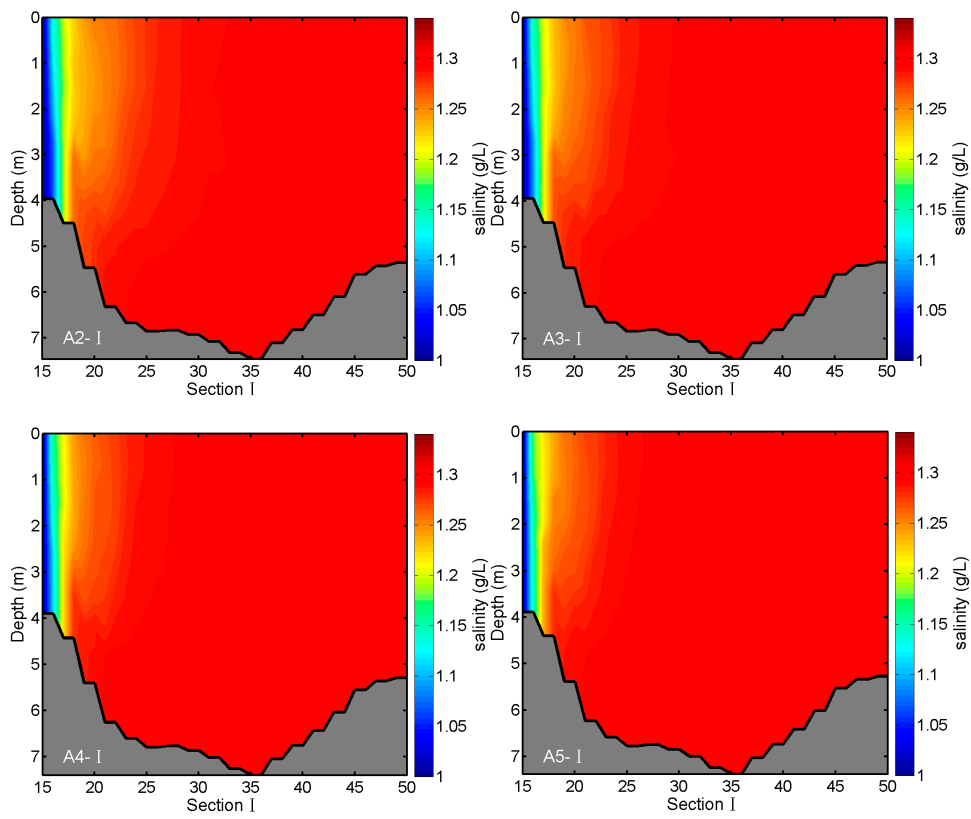
Figure 12. Distribution of modeled salinity at Section I in experiment (**A2-I**) A2, (**A3-I**) A3, (**A4-I**) A4, and (**A5-I**) A5.
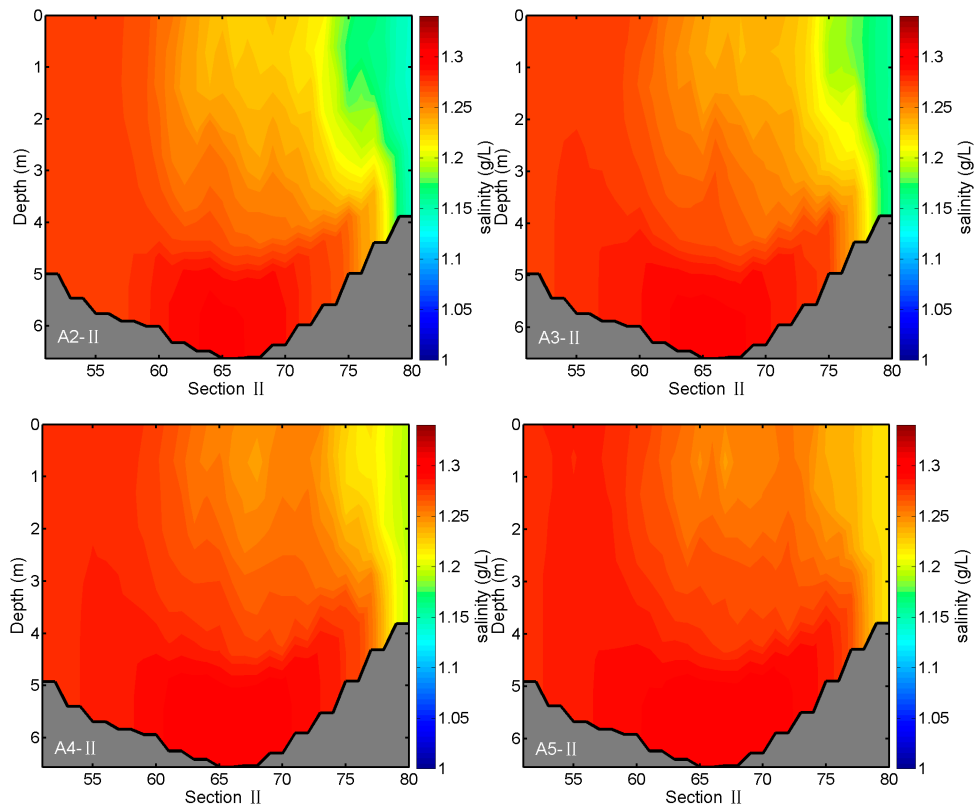
Figure 13. Distribution of modeled salinity at Section II in experiment (**A2- II**) A2, (**A3- II**) A3, (**A4- II**) A4, and (**A5- II**) A5.
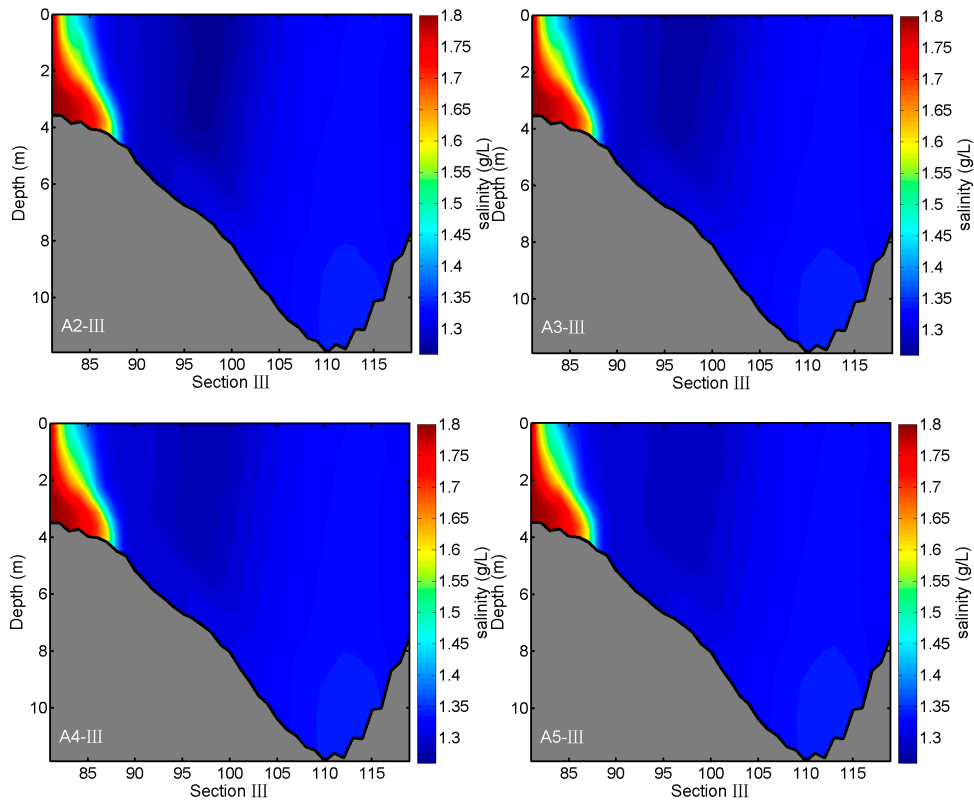
Figure 14. Distribution of modeled salinity at Section III in experiment (**A2-III**) A2, (**A3-III**) A3, (**A4-III**) A4, and (**A5-III**) A5.
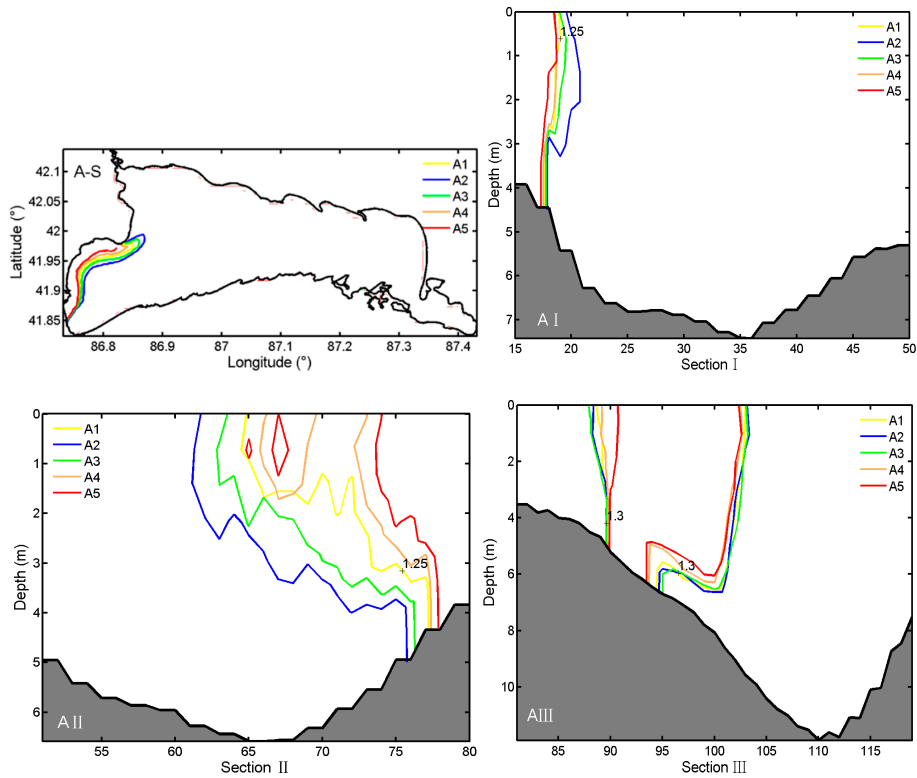
Figure 15. Comparison between the modeled 1.25 g L^{-1} isohalines at (**A-S**) surface, (**AI**) Section I, (**AII**) Section II, and 1.3 g L^{-1} isohalines at (**AIII**) Section III, in experiments A1, A2, A3, A4, and A5.

The salinity increased little at section III with the decrease in the discharge of Kaidu River (Figure 14). At section III, the salinity increased only in the middle of the section, for the region with salinity lower than 1.3 g L^{-1} was decreased (Figure 15(AIII)). The section III is influenced less by the discharge of Kaidu River, but due to the bank flow along the western bank and northeast flow, the freshwater from Kaidu River flows to the northeast of the lake, especially to the middle of the section III, so the salinity of the middle of section III increased with the decrease in the discharge of Kaidu River.

The salinity changes only at sites 10, 11, and 12 (Figure 1), with the decrease in the discharge of Kaidu River (Figure 16). This is also due to the flow along the western bank and in northeastward.
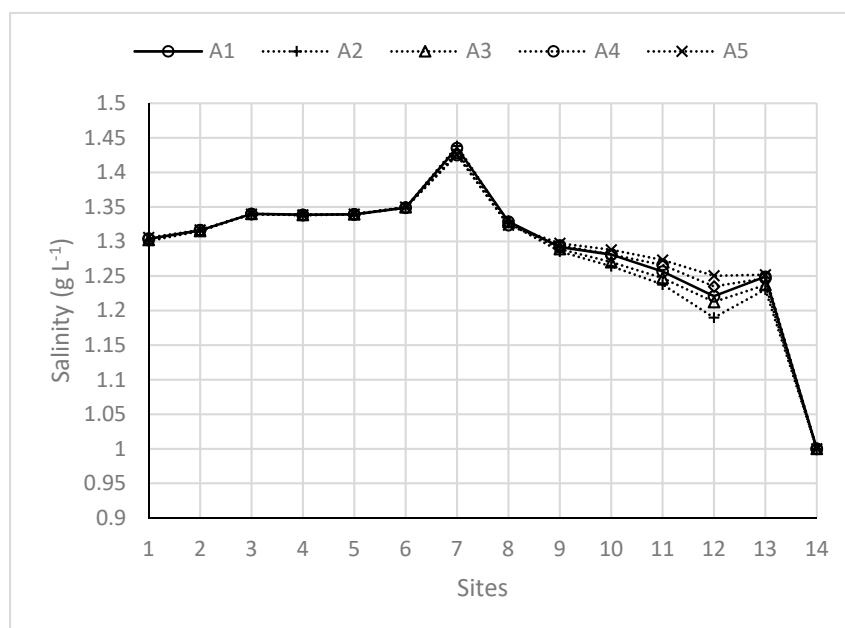
Figure 16. Comparison between the salinity of different sites in experiments A1, A2, A3, A4, and A5.

4. Conclusions

The effects of Kaidu River discharge on the salinity structure of Bosten Lake was studied by a three-dimensional numerical model: the Estuarine, Coastal, and Ocean Modeling System with Sediments (ECOMSED). The model used an orthogonal horizontal curvilinear grid of 550 m × 550 m and 11 equal thickness sigma (terrain-following) layers in the vertical direction. It was forced by atmospheric forcing obtained from the China Climatology Meteorological Data Sharing Service System and river discharges were obtained from the Hydrological Yearbook of People's Republic of China. The initial climatological temperature and salinity fields for the model were obtained from national controlled Environmental Monitoring Station. Kriging interpolation was applied to derive the initial fields for the required model specification. The modeled water level, temperature, and salinity were in reasonable conformity with the observed data, and the modeled currents were in conformity with the results of Han et al. (2004) [24]. The currents at the surface were mainly eastward, whilst those in the bottom layer were mainly westward. The simulated salinity was lowest in the southwestern part of the lake, especially from around the inlet of Kaidu River to its left along the western bank, highest in the northwestern part of the lake, especially from around the inlet of Huangshuigou to its left along the northern bank, and is of intermediate value in other regions, where the distribution of salinity is almost homogenous. A group of sensitivity experiments was processed to study the response of the salinity structure to changes in river discharges on 22 June. Due to the lake's flow pattern, changes in Kaidu River discharge have a great influence on the salinity structure of the southwest of Bosten Lake. The Kaidu River discharge mostly flowed northeastward along the western bank of the lake, so that with the decrease in Kaidu River discharge, the salinity of the region from the inlet of the river to its

right increased, based on salinity distribution or the location of specific isohalines of the surface, the bottom layer, and along the three transects. With the salinity spatial distribution information of Bosten Lake and its response to Kaidu River discharge, the proper management policy can be provided.

Author Contributions: Y.L. built the ECOMSED model of Bosten Lake and writing the original draft. A.B. supervised the research work. X.C. provided guidance and offered suggestions to improve the manuscript. R.Z. analyzed the data.

Conflicts of Interest: The authors declare no conflict of interest.

References

1. Schofield, N.J.; Ruprecht, J.K. Regional analysis of stream salinisation in southwest Western Australia. *J. Hydrogeol.* **1989**, *112*, 19–39. [CrossRef]
2. Zuo, Q.T.; Dou, M.; Chen, X.; Zhou, K.F. Physically-based model for studying the salinization of Bosten Lake in China. *Hydrol. Sci. J.* **2006**, *51*, 432–449. [CrossRef]
3. Williams, W.D. Anthropogenic salinisation of inland waters. *Hydrobiologia* **2001**, *466*, 329–337. [CrossRef]
4. Alcocer, J.; Escobar, E.; Lugo, A. Water use (and abuse) and its effects on the crater-lakes of Valle de Santiago, Mexico. *Lakes Reserv. Res. Manag.* **2000**, *5*, 145–149. [CrossRef]
5. Feng, Q.; Cheng, G.D. Current situation, problems and rational utilization of water resources in arid northwestern China. *J. Arid Environ.* **1998**, *40*, 373–382.
6. Migahid, M.M. Effect of salinity shock on some desert species native to the northern part of Egypt. *J. Arid Environ.* **2003**, *53*, 155–167. [CrossRef]
7. Tang, X.M.; Xie, G.J.; Shao, K.Q.; Bayartu, S.; Chen, Y.G.; Gao, G. Influence of salinity on the bacterial community composition in Lake Bosten, a large oligosaline lake in arid northwestern China. *Appl. Environ. Microb.* **2012**, *78*, 4748–4751. [CrossRef] [PubMed]
8. Williams, W.D. Salinisation: A major threat to water resources in the arid and semi-arid regions of the world. *Lakes Reserv. Res. Manag.* **1999**, *4*, 85–91. [CrossRef]
9. Bai, J.; Chen, X.; Li, J.L.; Yang, L.; Fang, H. Changes in the area of inland lakes in arid regions of central Asia during the past 30 years. *Environ. Monit. Assess.* **2011**, *178*, 247–256. [CrossRef]
10. Xie, G.J.; Zhang, J.; Tang, X.M.; Cai, Y.; Gao, G. Spatio-temporal heterogeneity of water quality and succession patterns in Lake Bosten during the past 50 years. *J. Lake Sci.* **2011**, *23*, 988–998.
11. Beaumont, P. Agricultural and environmental changes in the upper Euphrates catchment of Turkey and Syria and their political and economic implications. *Appl. Geogr.* **1996**, *16*, 137–157. [CrossRef]
12. Farber, E.; Vengosh, A.; Gavrieli, I.; Marie, A.; Bullen, T.D.; Mayer, B.; Holtzman, R.; Segal, M.; Shavit, U. The origin and mechanisms of salinization of the Lower Jordan River. *Geochim. Cosmochim. Acta* **2004**, *68*, 1989–2006. [CrossRef]
13. Gates, T.K.; Burkhalter, J.P.; Labadie, J.W.; Valliant, J.C.; Broner, I. Monitoring and modelling flow and salt transport in a salinity-threatened irrigated valley. *J. Irrig. Drain. Eng.* **2002**, *128*, 87–99. [CrossRef]
14. Kotb, T.H.S.; Watanabe, T.; Ogino, Y.; Tanji, K.T. Soil salinization in the Nile Delta and related policy issues in Egypt. *Agric. Water Manag.* **2000**, *43*, 239–261. [CrossRef]
15. Pillsbury, A.F. The salinity of rivers. *Sci. Am.* **1981**, *245*, 54–65. [CrossRef]
16. Robson, J.F.; Stoner, R.F.; Perry, J.H. Disposal of drainage water from irrigated alluvial plains. *Water Sci. Technol.* **1983**, *16*, 41–55. [CrossRef]
17. Xia, J.; Zuo, Q.T.; Shao, M.C. *Sustainable Management of Water Resources in Lake Bosten*; Chinese Science Press: Beijing, China, 2003.
18. Zhou, C.H.; Luo, G.P.; Li, C.; Tang, Q.C.; Li, H.G.; Wang, Q.M.; Fuikui, H. Environmental change in Bosten Lake and its relation with the oasis reclamation in Yanqi Basin. *Geogr. Res.* **2001**, *20*, 14–23.

19. Zuo, Q.T.; Chen, X. *Water Planning and Management Meeting Sustainable Development*; China Hydropower Press: Beijing, China, 2003.

20. Cheng, Z.C.; Li, Y.A. Water-salt equilibrium and mineralization of Bosten Lake, Xinjiang. *Arid Land Geogr.* **1997**, *20*, 43–49.

21. Dong, X.G.; Zhong, R.S.; Liu, F. Differentiation of Water-salt-interaction in Bostan Lake and Peacock River in Recent Fifty Year. *Sci. Technol. Rev.* **2006**, *24*, 34–37.

22. Wang, Y.J.; Li, Y.A.; Wang, Y.G.; Tan, Y. Study on the change of inflow and salt content of the Bosten Lake, Xinjiang since the 1950s. *Arid Zone Res.* **2005**, *22*, 355–360.

23. Zhao, J.F.; Qin, D.H.; Nagashima, H.; Lei, J.Q.; Wei, W.S. Analysis of mechanism of the salinization process and the salinity variation in Bosten Lake. *Adv. Water Sci.* **2007**, *18*, 475–482.

24. Han, L.X.; Zhang, F.X.; Zhang, P.; Liu, X.T. Flow field and salinity distribution of large inland lake. *J. Hydraul. Eng.* **2004**, *111*, 100–105.

25. Jiang, G.Q.; Hou, J.; Qiu, X.Y.; Zhou, Z. Numerical simulation of salinity in Bosten Lake. *Hydro-Sci. Eng.* **2002**, *1*, 40–43.

26. Li, Y.A.; Tan, Y.; Jiang, F.Q.; Wang, Y.J.; Hu, R.J. Study on hydrological features of the Kaidu River and the Bosten Lake in the second half of 20th century. *J. Glaciol. Geocryol.* **2003**, *25*, 215–218.

27. Cheng, Q.C. *Studies on Bosten Lake*; Hehai Unversity Press: Nan Jing, China, 1995.

28. Mischke, S. Holocene environmental fluctuations of Lake Bosten (Xinjiang, China) inferred from ostracods and stable isotopes. In Proceedings of the EGS-AGU-EUG Joint Assembly, Nice, France, 6–11 April 2003.

29. Wei, K.Y.; Lee, M.Y.; Wang, C.H.; Wang, Y.; Lee, T.Q.; Yao, P. Stable isotopic variations in oxygen and hydrogen of waters in Lake Bosten region, Southern Xinjiang, Western China. *West. Pac. Earth Sci.* **2002**, *2*, 67–82.

30. Jiu, X.; Liu, H.; Tu, Q.; Zhang, Z.; Zhu, X. (Eds.) *Eutrophication of Lakes in China (The 4th International Conference on the Conservation and Management of Lakes "Hangzhou 90")*; The Conference: Hangzhou, China, 1990; 652p.

31. Zhang, G.; Xu, N.; Mecuthon, S.; Yang, Q.; Li, Y.; Zhou, W. Lake Bosten in Uygur Autonomous Region of Xinjiang. In *Lakes in China: Research of Their Environment*; Jin, X., Ed.; China Ocean Press: Beijing, China, 1995; Volume I.

32. Xu, H.L.; Guo, Y.P.; Li, W.H. Analysis on the water pollution in Bosten Lake, Xinjiang. *Arid Zone Res.* **2003**, *20*, 192–196.

33. Blumberg, A.F.; Mellor, G.L. A Description of a Three-Dimensional Coastal Ocean Circulation Model. In *Three-Dimensional Coastal Ocean Models*; Heaps, N., Ed.; American Geophysical Union: Washington, DC, USA, 1987; pp. 1–16.

34. Blumberg, A.F. An Estuarine and Coastal Ocean Version of POM. In Proceedings of the Princeton Ocean Model Users Meeting (POM96), Princeton, NJ, USA, 10–12 June 1996.

35. Mellor, G.L.; Yamada, T. Development of a turbulence closure model for geophysical fluid problems. *Rev. Geophys. Space Phys.* **1982**, *20*, 851–875. [CrossRef]

36. Blumberg, A.F. *A Primer for ECOMSED, Version 1.3*; User's Manual; HydroQual Inc.: Mahwah, NJ, USA, 2002.

37. Blumberg, A.F.; Mellor, G.L. A coastal ocean numerical model. In *Mathematical Modelling of Estuarine Physics*; Springer: New York, NY, USA, 1980.

38. Smagorinsky, J. General Circulation Experiments with the Primitive Equations, I. The Basic Experiment. *Mon. Weather Rev.* **1963**, *91*, 99–164. [CrossRef]

39. Ahsan, A.K.M.Q.; Blumberg, A.F. A three-dimensional hydrothermal model of Onondaga Lake, New York. *J. Hydraul. Eng.* **1999**, *125*, 912–923. [CrossRef]

40. Rosati, A.; Miyakoda, K. A general circulation model for upper ocean simulation. *J. Phys. Oceanogr.* **1988**, *18*, 1601–1626. [CrossRef]

41. SLB. *Hydrological Yearbook of the People's Republic of China of Inland Rivers and Lakes in the Southern Tian-Shan Mountains*; SLB: Xinjiang, China; Beijing, China, 2005.